LBL-31804
Preprint

Lawrence Berkeley Laboratory
UNIVERSITY OF CALIFORNIA

Physics Division

Mathematics Department

To be submitted for publication

A Three-Dimensional Adaptive Vortex Method and Its Applications to the Study of Nonlinear Waves on Vortex Filaments

A. Qi

February 1992

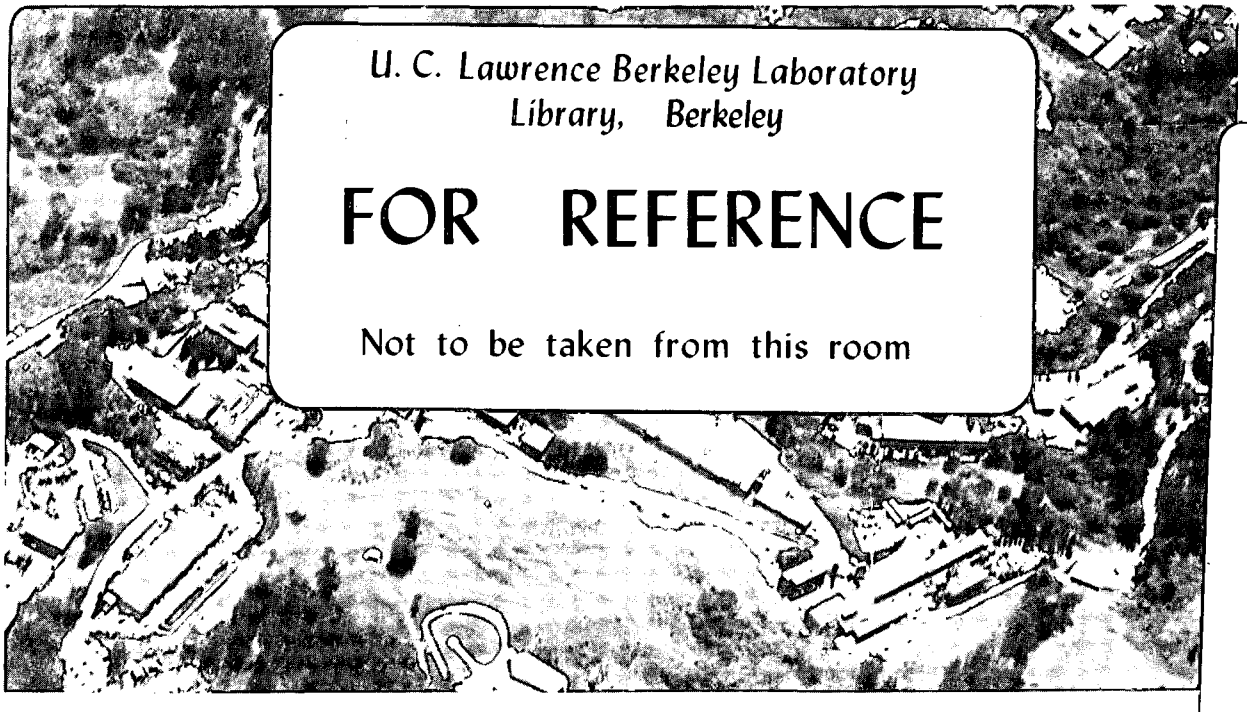

U. C. Lawrence Berkeley Laboratory
Library, Berkeley

FOR REFERENCE

Not to be taken from this room

LBL-31804
Copy 1
Bldg. 50 Library.

Prepared for the U.S. Department of Energy under Contract Number DE-AC03-76SF00098

DISCLAIMER

This document was prepared as an account of work sponsored by the United States Government. Neither the United States Government nor any agency thereof, nor The Regents of the University of California, nor any of their employees, makes any warranty, express or implied, or assumes any legal liability or responsibility for the accuracy, completeness, or usefulness of any information, apparatus, product, or process disclosed, or represents that its use would not infringe privately owned rights. Reference herein to any specific commercial product, process, or service by its trade name, trademark, manufacturer, or otherwise, does not necessarily constitute or imply its endorsement, recommendation, or favoring by the United States Government or any agency thereof, or The Regents of the University of California. The views and opinions of authors expressed herein do not necessarily state or reflect those of the United States Government or any agency thereof or The Regents of the University of California and shall not be used for advertising or product endorsement purposes.

Lawrence Berkeley Laboratory is an equal opportunity employer.

DISCLAIMER

This document was prepared as an account of work sponsored by the United States Government. While this document is believed to contain correct information, neither the United States Government nor any agency thereof, nor the Regents of the University of California, nor any of their employees, makes any warranty, express or implied, or assumes any legal responsibility for the accuracy, completeness, or usefulness of any information, apparatus, product, or process disclosed, or represents that its use would not infringe privately owned rights. Reference herein to any specific commercial product, process, or service by its trade name, trademark, manufacturer, or otherwise, does not necessarily constitute or imply its endorsement, recommendation, or favoring by the United States Government or any agency thereof, or the Regents of the University of California. The views and opinions of authors expressed herein do not necessarily state or reflect those of the United States Government or any agency thereof or the Regents of the University of California.

LBL-31804

A THREE-DIMENSIONAL ADAPTIVE VORTEX METHOD AND ITS APPLICATIONS TO THE STUDY OF NONLINEAR WAVES ON VORTEX FILAMENTS *

Anmin Qi

Lawrence Berkeley Laboratory
and
Department of Mathematics
University of California
Berkeley, CA 94720

February, 1992

* This work was supported in part by the Applied Mathematical Sciences subprogram of the Office of Energy Research, U.S. Department of Energy under Contract DE-AC03-76SF00098, and in part by the National Science Foundation under grant number DMS89-19074.

List of Figures

1 The vortex segments 3
2 Think of three parts in computation for a long vortex tube 5
3 The partition of initial data. 7
4 An numerical experiment — Scheme 2 produces error perturbed waves on vortex filaments 11
5 Trace the wave. 12
6 Perspective view of a space curve describing a solitary wave on a vortex filament 13
7 A solitary wave propagation on a vortex filament. 16
8 Collision of two solitons on a vortex filament. 18

Abstract

A vortex method is one of the main numerical tools in the study of incompressible fluid flow. With a regular three dimensional vortex method, one can follow the evolution of a particular part of a vortex tube, but can not trace a perturbed wave on a vortex tube unless one uses a large amount of computer memory. In this work, we present a three-dimensional adaptive vortex method which can be used to trace a wave accurately with use of a limited amount of computer memory. A successful application of the method to the study of solitons propagation on vortex filaments will be shown.

1 Introduction

Vortex methods have been used successfully to simulate various incompressible vortex flow phenomena in three dimensional space [6, 15, 13]. The methods follow the evolution of a vorticity field in the Lagrangian coordinates. One discretizes a vorticity field based on the fact that vortices are concentrated on some regions in the three dimensional space. Thus a vortex method follows a particular material volume which contains concentrated vortices.

We are often interested the wave phenomena on a concentrated vortex tube or vortex sheet. The studies of those wave phenomena on vorticity field provide important information to understand the vortex dynamics. The vortex stretching and nonlinear waves such as soliton on vortex line themselves are very interesting wave phenomena and have drawn a great attention for scientists whose work relates to fluid phenomena. The studies of vortex stretching and nonlinear waves on vorticity field are among the frontiers of modern science. A three dimensional vortex method is a good candidate to be used for study of the wave phenomena on a concentrated vorticity field. However, a wave is usually not confined in a given material volume. This is a problem in use of a vortex method for the study of wave phenomena on vorticity field. One can solve this problem by considering a large region which can guarantee the containment of the studied wave in whole computation. That is not always feasible because of the limited machine memory of today's computer.

In this work, we present a three dimensional adaptive wave tracing vortex method. Using this method, we are able to study a wave phenomenon on a concentrated vortex tube with a great accuracy without use of a large amount of computer memory.

A solitary wave is a nonlinear wave with permanent form whose tails approach a constant at infinity. A soliton is a solitary wave that can interact strongly with other solitons and retain its identity. A soliton solution was first discovered for the KdV equation. We now knew that besides the KdV equation, the Sine-Gordon

equation and the nonlinear Schrödinger equation possess soliton solutions. (See Lamb [14] and Drazin & Johnson [7].)

On a vortex filament, Hasimoto first obtained a solitary wave solution for the localized induction approximation (LIA) of the Biot-Savart law [10]. He proved that the LIA is equivalent to the nonlinear Schrödinger equation.

However, the Euler equations which describe the motion of Euler flow are very different than the LIA in the sense that the LIA does not represent the vortex stretching [5]. To answer the question whether there are solitons in the Euler flow, physical and numerical experiments have been conducted. In physical experiments, Hopfinger, Browand & Gagne [11] and Maxwathy, Hopfinger & Redekopp [16] reported the appearance of solitons. The numerical experiments, on the other hand, was not very successful [1].

Now, using the newly developed adaptive vortex scheme, we attempt again to search a solitary wave or solitons on a vortex filament numerically. The result is very satisfactory. We have successfully simulated a solitary wave propagation on a vortex filament and the strong interaction of two solitons.

In Section 2, a regular three dimensional vortex filament method is described. In Section 3, an adaptive vortex method algorithm is given. A detailed analysis and proper treatment of a numerical error that could be generated by the algorithm are also described here. In Section 4, the simulations of a solitary wave propagation and the interaction of two solitons on a vortex filaments are demonstrated. Although the results displayed in this work only for one filament, we have tested these simulations on up to five filaments with very similar outputs. Finally, Section 5 will be devoted to a summary and further discussion.

2 The Basic 3-D Vortex Methods Scheme

The velocity field $\mathbf{u}(\mathbf{x},t) = (u,v,w)$ of the incompressible, inviscid fluid flows is described by the Euler equations

$$\frac{D\mathbf{u}}{Dt} = \frac{\partial \mathbf{u}}{\partial t} + (\mathbf{u}\cdot\nabla)\mathbf{u} = -\nabla P \tag{1}$$

$$\nabla\cdot\mathbf{u} = 0 \tag{2}$$

Where $\mathbf{x} = (x,y,z)$ is the position, t time, P pressure and $\nabla = (\partial/\partial x, \partial/\partial y, \partial/\partial z)$

Define the *vorticity* $\boldsymbol{\omega}$,

$$\boldsymbol{\omega} = \nabla\times\mathbf{u}$$

Taking curl of equation (1), we have the vorticity transport equation

$$\frac{\partial\boldsymbol{\omega}}{\partial t} + (\mathbf{u}\cdot\nabla)\boldsymbol{\omega} = (\boldsymbol{\omega}\cdot\nabla)\mathbf{u} \tag{3}$$

From equations (2) and (3), one can find a integral form of velocity $\mathbf{u}$ in terms of $\boldsymbol{\omega}$:

$$\mathbf{u} = -\frac{1}{4\pi}\int_{R^3} \frac{(\mathbf{x}-\mathbf{x}')\times\boldsymbol{\omega}(\mathbf{x}')d\mathbf{x}'}{|\mathbf{x}-\mathbf{x}'|^3} \tag{4}$$

On a vortex filament C, equation (4) can be written as

$$\mathbf{u}(\mathbf{x},t) = -\frac{\Gamma}{4\pi}\int_C \frac{(\mathbf{x}-\mathbf{x}')\times d\mathbf{l}(\mathbf{x}')}{|\mathbf{x}-\mathbf{x}'|^3} \tag{5}$$

where Γ is the circulation of C, $d\mathbf{l}$ is an infinitesimal material line element. This is the Biot-Sarvat law.

We like to evaluate the motion of vortex filament C. Integral equation (5) is not suitable for the numerical computation because it diverges with rate $1/|\mathbf{x}-\mathbf{x}'|^2$ if $\mathbf{x}$ is a point on curve C.

One can modify integral equation (5),

$$\mathbf{u}_\sigma(\mathbf{x},t) = -\frac{\Gamma}{4\pi}\int_C f(\frac{|\mathbf{x}-\mathbf{x}'|}{\sigma})\frac{(\mathbf{x}-\mathbf{x}')\times d\mathbf{l}(\mathbf{x}')}{|\mathbf{x}-\mathbf{x}'|^3} \tag{6}$$

where f is called a core function and σ a core size. In this work, we used a fourth order core function

$$f(r) = \tanh r^3 + \frac{3}{2}r^3\mathrm{sech}^2 r^3$$

which was proposed by Beale & Majda[4].

For an infinite long vortex filament, we divide it into segments. For the jth segment, the two ends are the points $\mathbf{x}_j$ and $\mathbf{x}_{j+1}$. Let $\delta\mathbf{l}_j = \mathbf{x}_{j+1} - \mathbf{x}_j$. (See Figure 1.).

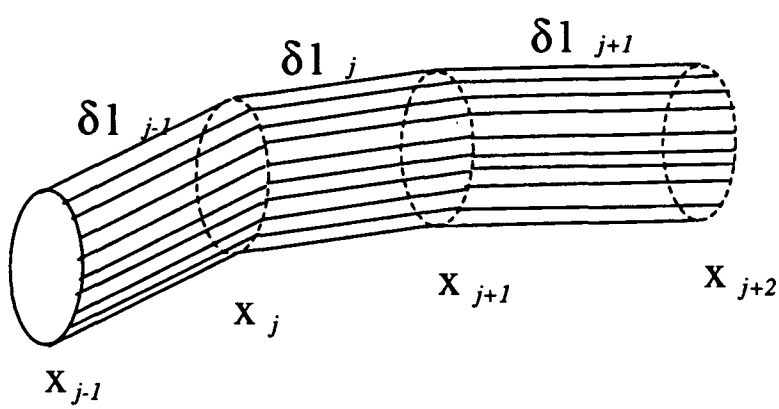

Figure 1: The vortex segments

Integral equation (6) can be written as

$$\mathbf{u}_\sigma(\mathbf{x},t) = -\frac{\Gamma}{4\pi}\sum_{j=-\infty}^{\infty}\int_{\delta\mathbf{l}_j} \frac{(\mathbf{x}-\mathbf{x}')\times d\mathbf{l}(\mathbf{x}')}{|\mathbf{x}-\mathbf{x}'|^3} f(\frac{|\mathbf{x}-\mathbf{x}'|}{\sigma}) \tag{7}$$

We require $|\delta \mathbf{l}_j| \leq h$ for all j where h is a predetermined small number. Thus

$$\int_{\delta \mathbf{l}_j} \frac{(\mathbf{x}-\mathbf{x}') \times d\mathbf{l}(\mathbf{x}')}{|\mathbf{x}-\mathbf{x}'|^3} f(\frac{|\mathbf{x}-\mathbf{x}'|}{\sigma}) \approx \frac{\mathbf{r}_j \times \delta \mathbf{l}_j}{r_j^3} f(\frac{r_j}{\sigma}) \tag{8}$$

where

$$\begin{aligned} \mathbf{r}_j &= \mathbf{x} - \tfrac{1}{2}(\mathbf{x}_{j+1} + \mathbf{x}_j) \\ r_j &= |\mathbf{r}_j| \end{aligned}$$

Inserting (8) into (7), we find

$$\mathbf{u}_\sigma(\mathbf{x},t) = -\frac{\Gamma}{4\pi} \sum_{j=-\infty}^{\infty} \frac{\mathbf{r}_j \times \delta \mathbf{l}_j}{r_j^3} f(\frac{r_j}{\sigma}) \tag{9}$$

Knowing $\mathbf{u}_\sigma$, we solve the ordinary differential equations

$$\frac{d\mathbf{x}}{dt} = \mathbf{u}_\sigma(\mathbf{x},t) \tag{10}$$

and we can determine the position of $\mathbf{x}_j$ at the next time $t+\Delta t$. There are various numerical methods to solve equation (10), for example, the second-order Heun method and the fourth-order Runge-Kutta method. We used the fourth-order Runge-Kutta method in this work,

$$\begin{aligned} \mathbf{x}_i^{(1)} &= \mathbf{x}_i(t) + \tfrac{\Delta t}{2}\mathbf{u}_\sigma(\mathbf{x}_i,t) \\ \mathbf{x}_i^{(2)} &= \mathbf{x}_i(t) + \tfrac{\Delta t}{2}\mathbf{u}_\sigma(\mathbf{x}_i^{(1)},t+\tfrac{\Delta t}{2}) \\ \mathbf{x}_i^{(3)} &= \mathbf{x}_i(t) + \Delta t\mathbf{u}_\sigma(\mathbf{x}_i^{(2)},t+\tfrac{\Delta t}{2}) \\ \mathbf{x}_i(t+\Delta t) &= \mathbf{x}_i(t) + \tfrac{\Delta t}{6}[\mathbf{u}_\sigma(\mathbf{x}_i,t) + 2\mathbf{u}_\sigma(\mathbf{x}_i^{(1)},t+\tfrac{\Delta t}{2}) \\ &\qquad + 2\mathbf{u}_\sigma(\mathbf{x}_i^{(2)},t+\tfrac{\Delta t}{2}) + \mathbf{u}_\sigma(\mathbf{x}_i^{(3)},t+\Delta t)] \end{aligned}$$

$\delta \mathbf{l}_j$ and the amount of vorticity carried by this vortex element grows as the vortex filament stretches. In order to maintain the partition fine enough for accurate computation, we split a segment $\delta \mathbf{l}_j$ into two with equal length if $|\delta \mathbf{l}_j| > h$. The time step Δt is determined by

$$\Delta t \max_j |\mathbf{u}_j^n| \leq K$$

where K is a given constant, $\mathbf{u}_j^n = \mathbf{u}_\sigma(\mathbf{x}_j(t^n),t^n)$, and t^n is the time at step n.

To simulate a thick vortex tube, one has to use several filaments in the computation, say M filaments. (See Qi [19, 18] for the explanation). In this case, we can rewrite equation (6) as follows:

$$\mathbf{u}_\sigma(\mathbf{x},t) = \sum_{m=1}^{M} \Gamma^{(m)} \int_{C_m} K_{\sigma_m}(\mathbf{x}(t)-\mathbf{x}'(t)) \times d\mathbf{l}(t)$$

Notice that for different filament, the circulation and core size may be chosen differently. Then the numerical scheme is

$$\mathbf{u}_\sigma(\mathbf{x},t) = -\frac{1}{4\pi}\sum_{m=1}^{M}\Gamma^{(m)}\sum_{j=-\infty}^{\infty}\frac{\mathbf{r}_j^{(m)}\times\delta\mathbf{l}_j^{(m)}}{(r_j^{(m)})^3}f(\frac{r_j^{(m)}}{\sigma}) \tag{11}$$

where $\sigma = \sigma_m$ if $\mathbf{x}$ is not on any given filament and $\sigma = (\frac{\sigma_m^2+\sigma_l^2}{2})^{1/2}$ or $\sigma = (\sigma_m\sigma_l)^{1/2}$ if $\mathbf{x}$ is on the lth filament; σ_m may also be varied with time or with arc length and time to conserve volume.

We must truncate the terms far away from the given point $\mathbf{x}$ in the schemes (9) and (11). Actually, we pick up a large number N replacing the infinity for all $\mathbf{x}$ in the real computation. In doing this, we compute only a part of an infinite long vortex filament. We must carefully deal with points near or at the truncated ends. There are two different cases:

1. the data are periodic;
2. the data are not periodic.

The first case is assumed in most of vortex computations, see, for example, Chorin [6], Leonard [15] and Knio & Ghoniem [13]. The second case is considered in this work because of the nature of physical phenomena which we are attempting to simulate. We assume that there is no disturbance at the place far away from the part computed. Therefore, we can extend each filament at the truncated ends with straight lines. (See Qi [19, 18] for detailed explanation). We can hence think of three parts in our computation for both cases. The middle part is evaluated and other two parts are determined by the nature of our data and the values of the middle part. (See Figure 2.)

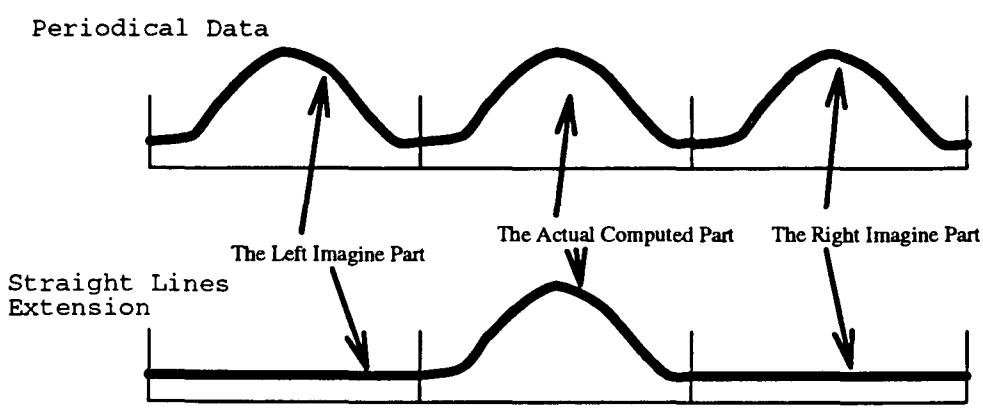

Figure 2: Think of three parts in computation for a long vortex tube

We must include the left and the right parts in our computation. Thus the scheme we used in our computation is:

$$
\begin{aligned}
\mathbf{u}_\sigma(\mathbf{x},t) = & - \frac{1}{4\pi}\sum_{m=1}^{M}\Gamma^{(m)}\sum_{j=-N_m}^{N_m}\left[\frac{\mathbf{r}_j^{(m)}\times\delta\mathbf{l}_j^{(m)}}{(r_j^{(m)})^3}f(\frac{r_j^{(m)}}{\sigma})\right. \\
& + \frac{\tilde{\mathbf{r}}_j^{(m)}\times\delta\mathbf{l}_j^{(m)}}{(\tilde{r}_j^{(m)})^3}f(\frac{\tilde{r}_j^{(m)}}{\sigma}) \\
& + \left.\frac{\bar{\mathbf{r}}_j^{(m)}\times\delta\mathbf{l}_j^{(m)}}{(\bar{r}_j^{(m)})^3}f(\frac{\bar{r}_j^{(m)}}{\sigma})\right]
\end{aligned}
$$

where

$$
\begin{aligned}
\mathbf{r}_j &= \mathbf{x} - \tfrac{1}{2}(\mathbf{x}_{j+1}+\mathbf{x}_j) \\
\tilde{\mathbf{r}}_j &= \mathbf{x} - \tfrac{1}{2}(\tilde{\mathbf{x}}_{j+1}+\tilde{\mathbf{x}}_j) \\
\bar{\mathbf{r}}_j &= \mathbf{x} - \tfrac{1}{2}(\bar{\mathbf{x}}_{j+1}+\bar{\mathbf{x}}_j) \\
r_j &= |\mathbf{r}_j| \\
\tilde{r}_j &= |\tilde{\mathbf{r}}_j| \\
\bar{r}_j &= |\bar{\mathbf{r}}_j|
\end{aligned}
$$

for the periodic data,

$$
\tilde{\mathbf{x}}_j = \begin{pmatrix} x_{N+1}+x_j-x_1 \\ y_j \\ z_j \end{pmatrix} \quad \bar{\mathbf{x}}_j = \begin{pmatrix} x_1-(x_{N+1}-x_j) \\ y_j \\ z_j \end{pmatrix}
$$

for the straight lines extension,

$$
\tilde{\mathbf{x}}_j = \begin{pmatrix} 2\tilde{x}_{j-1}-\tilde{x}_{j-2} \\ y_{N+1} \\ z_{N+1} \end{pmatrix} \quad \bar{\mathbf{x}}_j = \begin{pmatrix} 2\bar{x}_{j-1}-\bar{x}_{j-2} \\ y_{N+1} \\ z_{N+1} \end{pmatrix}
$$

$$
\begin{aligned}
\tilde{x}_1 &= x_{N+1} \\
\tilde{x}_2 &= 2x_{N+1}-x_N \\
\bar{x}_1 &= x_1 \\
\bar{x}_2 &= 2x_1-x_2
\end{aligned}
$$

3 An Adaptive Scheme

Using the 3-D vortex method described above, we can trace the evolution of a particular part of a vortex tube, but we are not able to follow a perturbed wave on a vortex tube which often is what people want to do. Therefore we need to modify our 3-D vortex scheme so that we can follow a wave propagation on an

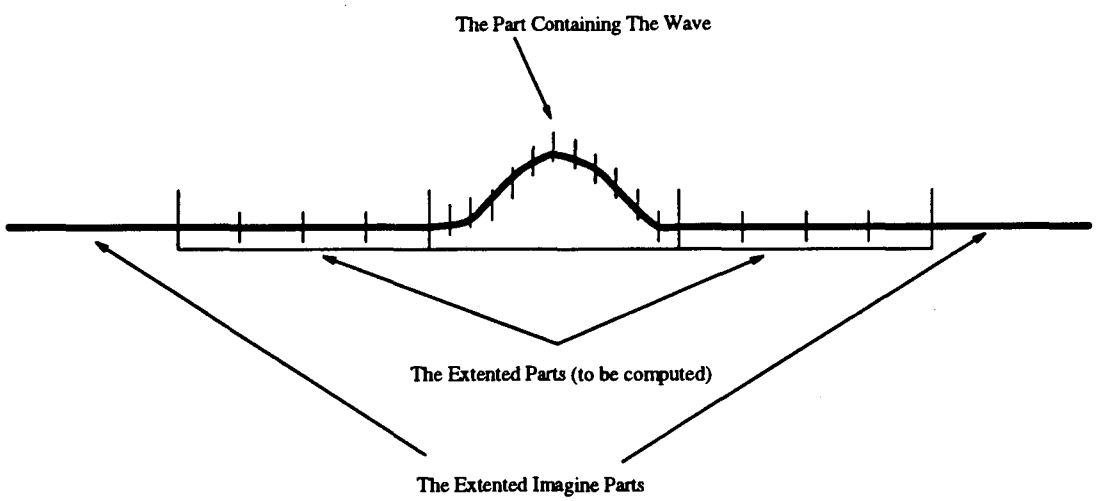

Figure 3: The partition of initial data.

infinite long vortex tube. The data are not periodic because we like to see how a particular shape of initial perturbed wave evolves along a straight vortex tube.

We divide a vortex tube to five parts this time. (see Figure 3.) The middle part contains the wave to be traced. For this part, we must use smaller length for each segment in our computation in order to gain a higher accuracy. We use longer length for the two parts next to the middle part. There are three reasons for computing these parts:

1. There are dispersive waves coming from the main wave spreading quickly to two sides of the main wave. We can not ignore them when they are close to the main part. One will see later the phenomena described here.
2. We need to know the motion outside the main part in order to trace the wave motion accurately. It is essential for multi-filaments simulation.
3. Using longer length, we can, in some sense, smooth out the high frequency dispersive wave. In other words, we can reduce the possible stretching on the vortex tube.

With finer partition on a line, we can capture waves with short wave length. However, the finer partition is, the bigger relative numerical truncation error for computing the length of each segment. That is, without increasing precision of floating point, finer partition may not necessarily give better solution. This is particularly true in the numerical simulation of waves with short wave length on a vortex tube because of the stretching and instability of a vortex tube. Therefore we should give not only the upper limit for the length of a segment but also the lower limit according to the floating point precision.

From our computational experiments, we observed that the waves with short wave length generally travels faster than the waves with long wave length on a vortex filament. If those short length waves are not main object to be traced, they will move out from the main part. Those, moving towards the direction which the traced wave goes, are important because their residue will effect our computation later. However, at this direction, when the main part moves, we glue several shorter segments to a long segment. This procedure gives us freedom to smooth out the high frequency waves (or waves with short wave length) by properly choosing new node for the long segment.

The length difference can also produces numerical error. The perturbed waves introduced by this error most likely form so-called hairpin structure at later time step computation. Such structure is the cause of the blow-up for most of turbulent flow computation. Therefore, proper control of the length of segments may reduce the hairpin structure in the computation, and may provide more accurate result. To understand the reason, we give detailed analysis for an infinite long straight vortex tube. We use M filaments simulate the tube. Divide each filament to equal length segments. For simplicity, we assume $\Gamma^{(m)}/4\pi = 1$, $m = 1, \cdots, M$, and define $g(r) = f(\frac{r}{\sigma})/r^3$. We use three different schemes computing the velocity field at point $\mathbf{x} = (x, y, z)$:

Scheme 1.

$$\mathbf{u}_\sigma(\mathbf{x}, t) = -\sum_{m=1}^{M} \left[\sum_{j=-\infty}^{-1} \mathbf{r}_j^{(m)} \times \delta\mathbf{l}_j^{(m)} g(r_j^{(m)}) + \sum_{j=0}^{\infty} \mathbf{r}_j^{(m)} \times \delta\mathbf{l}_j^{(m)} g(r_j^{(m)}) \right]$$

Scheme 2.

$$\mathbf{u}_\sigma^{(1)}(\mathbf{x}, t) = -\sum_{m=1}^{M} \left[\sum_{j=-\infty}^{-1} \mathbf{r}_{2j}^{'(m)} \times \delta\mathbf{l}_{2j}^{'(m)} g(r_{2j}^{'(m)}) + \sum_{j=0}^{\infty} \mathbf{r}_j^{(m)} \times \delta\mathbf{l}_j^{(m)} g(r_j^{(m)}) \right]$$

Scheme 3.

$$\mathbf{u}_\sigma^{(2)}(\mathbf{x}, t) = -\sum_{m=1}^{M} \left[\sum_{j=-\infty}^{-1} \mathbf{r}_{2j}^{'(m)} \times \delta\mathbf{l}_{2j}^{'(m)} g(r_{2j}^{'(m)}) + \sum_{j=0}^{\infty} \mathbf{r}_{2j}^{''(m)} \times \delta\mathbf{l}_{2j}^{''(m)} g(r_{2j}^{''(m)}) \right]$$

where

$$\begin{array}{lll}
\delta\mathbf{l}_j^{(m)} = \mathbf{x}_{j+1}^{(m)} - \mathbf{x}_j^{(m)}, & \mathbf{r}_j^{(m)} = \mathbf{x} - \frac{1}{2}(\mathbf{x}_{j+1}^{(m)} + \mathbf{x}_j^{(m)}), & r_j^{(m)} = |\mathbf{r}_j^{(m)}|, \\
\delta\mathbf{l}_{2j}^{'(m)} = \mathbf{x}_{2(j+1)}^{(m)} - \mathbf{x}_{2j}^{(m)}, & \mathbf{r}_{2j}^{'(m)} = \mathbf{x} - \frac{1}{2}(\mathbf{x}_{2(j+1)}^{(m)} + \mathbf{x}_{2j}^{(m)}), & r_{2j}^{'(m)} = |\mathbf{r}_{2j}^{'(m)}|, \\
\delta\mathbf{l}_{2j}^{''(m)} = \mathbf{x}_{2(j+1)}^{(m)} - \mathbf{x}_{2j}^{(m)}, & \mathbf{r}_{2j}^{''(m)} = \mathbf{x} - \frac{1}{2}(\mathbf{x}_{2(j+1)}^{(m)} + \mathbf{x}_{2j}^{(m)}), & r_{2j}^{''(m)} = |\mathbf{r}_{2j}^{''(m)}|.
\end{array}$$

Scheme 1 and scheme 3 have equal length segments. The length of segments for the third scheme is twice of the length for segments used in the first scheme.

Scheme 2 has two type of segments with different lengths. The length for the left side segments from point $\mathbf{x}_0$ is twice of the length for the right ones.

Since all $\delta\mathbf{l}_j^{(m)}$s have equal length and are parallel each other, we can write

$$\delta\mathbf{l}_j^{(m)} = \delta\mathbf{l}$$

where $\delta\mathbf{l}$ is a constant vector. Consequently,

$$\delta\mathbf{l}_{2j}^{'(m)} = \delta\mathbf{l}_{2j}^{''(m)} = 2\delta\mathbf{l}.$$

The schemes can be re-written as follows,

Scheme 1.

$$\mathbf{u}_\sigma(\mathbf{x},t) = -\left[\sum_{m=1}^{M}\left(\sum_{j=-\infty}^{-1}\mathbf{r}_j^{(m)}g(r_j^{(m)}) + \sum_{j=0}^{\infty}\mathbf{r}_j^{(m)}g(r_j^{(m)})\right)\right] \times \delta\mathbf{l}$$

Scheme 2.

$$\mathbf{u}_\sigma^{(1)}(\mathbf{x},t) = -\left[\sum_{m=1}^{M}\left(2\sum_{j=-\infty}^{-1}\mathbf{r}_{2j}^{'(m)}g(r_{2j}^{'(m)}) + \sum_{j=0}^{\infty}\mathbf{r}_j^{(m)}g(r_j^{(m)})\right)\right] \times \delta\mathbf{l}$$

Scheme 3.

$$\mathbf{u}_\sigma^{(2)}(\mathbf{x},t) = -2\left[\sum_{m=1}^{M}\left(\sum_{j=-\infty}^{-1}\mathbf{r}_{2j}^{'(m)}g(r_{2j}^{'(m)}) + \sum_{j=0}^{\infty}\mathbf{r}_{2j}^{''(m)}g(r_{2j}^{''(m)})\right)\right] \times \delta\mathbf{l}$$

Let us compute $\mathbf{u}_\sigma(\mathbf{x},t) - \mathbf{u}_\sigma^{(2)}(\mathbf{x},t)$ and $\mathbf{u}_\sigma(\mathbf{x},t) - \mathbf{u}_\sigma^{(1)}(\mathbf{x},t)$,

$$\begin{aligned}
\mathbf{u}_\sigma(\mathbf{x},t) - \mathbf{u}_\sigma^{(2)}(\mathbf{x},t) &= \left\{\sum_{m=1}^{M}\left[2\left(\sum_{j=-\infty}^{-1}\mathbf{r}_{2j}^{'(m)}g(r_{2j}^{'(m)}) + \sum_{j=0}^{\infty}\mathbf{r}_{2j}^{''(m)}g(r_{2j}^{''(m)})\right)\right.\right. \\
&\quad \left.\left. - \left(\sum_{j=-\infty}^{-1}\mathbf{r}_j^{(m)}g(r_j^{(m)}) + \sum_{j=0}^{\infty}\mathbf{r}_j^{(m)}g(r_j^{(m)})\right)\right]\right\} \times \delta\mathbf{l} \\
\mathbf{u}_\sigma(\mathbf{x},t) - \mathbf{u}_\sigma^{(1)}(\mathbf{x},t) &= \left\{\sum_{m=1}^{M}\left[2\sum_{j=-\infty}^{-1}\mathbf{r}_{2j}^{'(m)}g(r_{2j}^{'(m)}) - \sum_{j=-\infty}^{-1}\mathbf{r}_j^{(m)}g(r_j^{(m)})\right]\right\} \times \delta\mathbf{l}
\end{aligned}$$

For $\mathbf{x} = (x_{2k}, y, z)$, $k = \pm 1, \pm 2, \cdots$, y and z are arbitrary value, by symmetry,

$$r_{-2(j+1)+2k}^{'(m)} = r_{2j+2k}^{''(m)}, \quad r_{-j-1+2k}^{(m)} = r_{j+2k}^{(m)}$$

and both $\mathbf{r}_{-2(j+1)+2k}^{'(m)} + \mathbf{r}_{2j+2k}^{''(m)}$ and $\mathbf{r}_{-j-1+2k}^{(m)} + \mathbf{r}_{j+2k}^{(m)}$ have zero x components. Thus $\mathbf{u}_\sigma(\mathbf{x},t) - \mathbf{u}_\sigma^{(2)}(\mathbf{x},t)$ does not depend on x component of $\mathbf{x}$. Therefore, the velocity

difference between scheme 1 and scheme 3 are uniform on whole line $C = \{\mathbf{x} = (x, y_C, z_C) : -\infty < x < \infty, \ y_C$ and z_C are constants$\}$ which is parallel to the vortex tube. However, $\mathbf{u}_\sigma(\mathbf{x}, t) - \mathbf{u}_\sigma^{(1)}(\mathbf{x}, t)$ does depend on the x component of $\mathbf{x}$. Thus using scheme 2, one will get slight disturbance for the computed velocity field on the line C at or near the boundary of two different regions at each step. The accumulation of the local error gives us a big trouble for our numerical computation. Figure 4 shows an example that perturbed waves generated at boundaries of different regions by Scheme 2. In this example, we used four filaments to simulate an infinite long vortex tube. There are three computed parts. The middle part consists of segments with half length of the segments at two sides parts. The problem was solved in our computation by following means: using cubic spline interpolation, at or near a boundary of two regions, we divide those long segments to smaller ones with lengths approximately equal to those original short segments. Then we compute velocities at end points of the original segments with the newly generated short segments. For points far away from the boundaries, we use original segments to compute their velocity. The treatment is based on the locality of the problem. The result is satisfactory.

The adaptive and wave tracing vortex filament method algorithm is given as follows:

Step 1. Compute the initial data, i.e., chop the vortex tube to segments with different length according to where a segment locates.

Step 2. Compute velocity at the two end points of each segment. Here we must carefully deal with the points at or near the boundaries of different regions.

Step 3. Solve the ordinary differential equation $\frac{d\mathbf{x}}{dt} = \mathbf{u}$ to determine the position at next time step for each segment.

Step 4. Measure the motion of traced wave, i.e., determine the direction and length of the wave motion by comparing the new position of the wave to the position of the wave at the previous time step.

Step 5. Move the main part in where the traced wave is included, so that the traced wave stays in the middle of the newly determined main part.
<u>Method to move the main part:</u>
We want to keep the original segments on main part as much as possible because they are more accurate. That means we only want to add or delete some segments at two ends of the main part according to the measurement made at previous step. (See Figure 5.)

Step 6. We also need to add or drop segments at the ends of two parts next to main part according to the measurement made at step 4. (See Figure 5.)

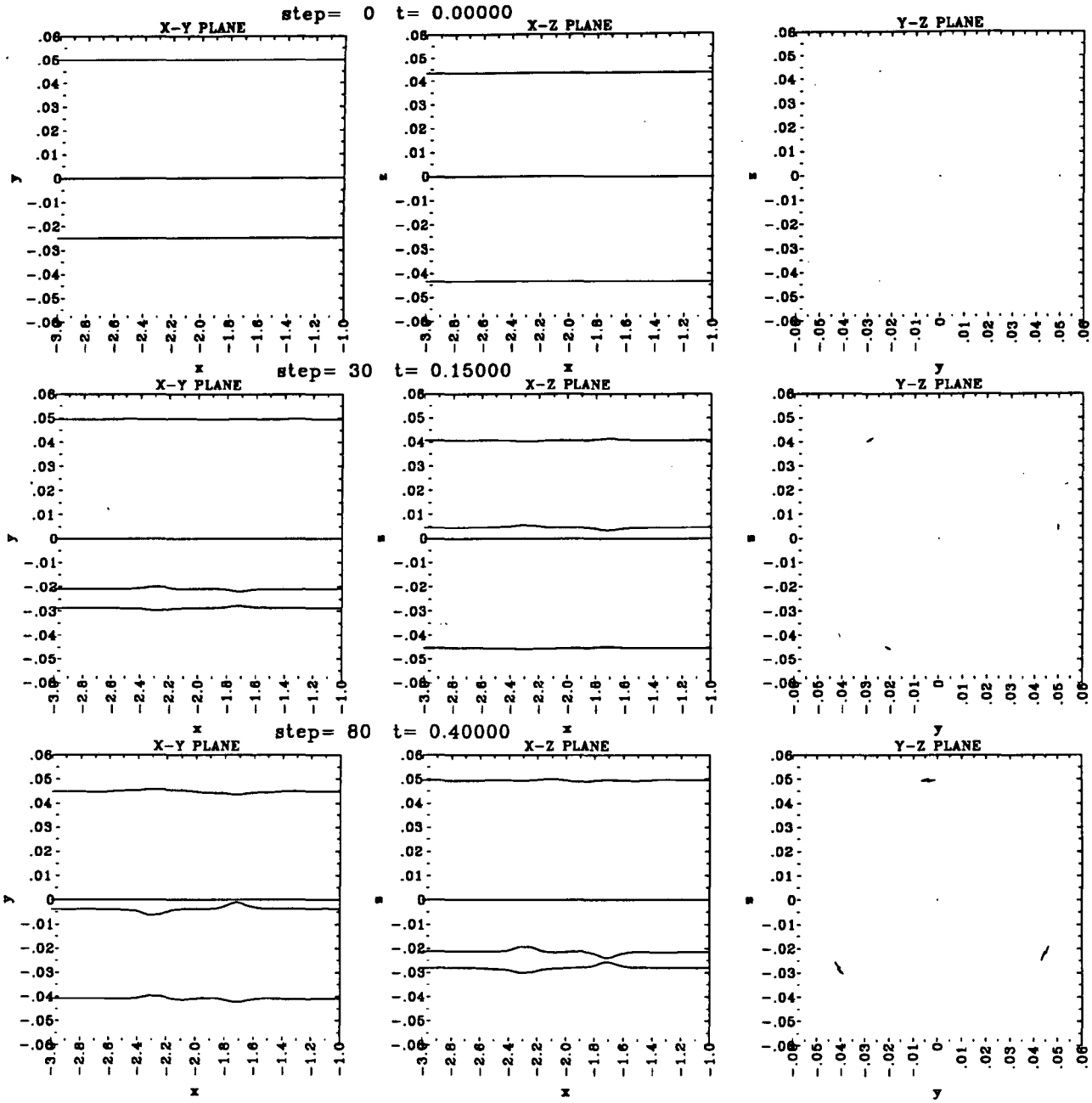

Figure 4: An numerical experiment — Scheme 2 produces error perturbed waves on vortex filaments

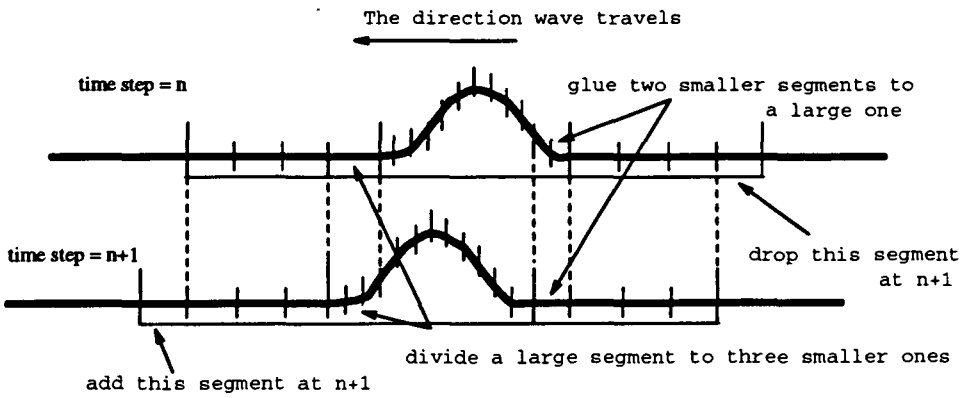

Figure 5: Trace the wave.

Step 7. Go to **Step 2.**

4 Solitons on a vortex tube - an application

The initial motivation of the development of the method described above was to study the solitary wave propagation on vortex tube.

A solitary wave solution on a vortex filament was found analytically for the localized induction approximation (LIA) of the Biot-Sarvat law (5) by Hasimoto [10, 1972].

The localized induction approximation

$$\frac{\partial \mathbf{x}}{\partial t} = \frac{\Gamma\kappa}{4\pi}[\ln\frac{L}{\varrho}]\mathbf{b} \tag{12}$$

is the leading order induction term for the Biot-Sarvat law (5). This approximation was derived by Arms and Hama. (See Hama [8, 9] and Arms & Hama [2]. See also Batchelor [3, p.509] for detailed derivation.) Here $\mathbf{x} = \mathbf{x}(s,t)$ is a point near the filament as a function of arc length s and time t, κ the curvature of the filament, $\mathbf{b}$ the unit binormal vector, L the length of the part whose contribution to the induced velocity is considered, and ϱ the distance between $\mathbf{x}$ and the filament. The approximation is correct only if $\frac{L}{\varrho} \to \infty$

Assuming $\frac{L}{\varrho}$ a constant and rescaling the time t, equation (12) becomes

$$\mathbf{x}_t = \mathbf{x}_s \times \mathbf{x}_{ss} \tag{13}$$

By use of the transformation

$$\psi = \kappa \exp(i \int_0^s \tau d\zeta)$$

Hasimoto proved that the LIA (13) is equivalent to the nonlinear Schrödinger equation

$$\frac{1}{i}\frac{\partial\psi}{\partial t} = \frac{\partial^2\psi}{\partial s^2} + \frac{1}{2}\psi(|\psi|^2 + A) \tag{14}$$

and obtained a curvature function of a solitary wave

$$\kappa(s,t) = 2\beta\mathrm{sech}[\beta(s - ct)] \tag{15}$$

for constant torsion $\tau = c/2$, where $\beta = \sqrt{A}/2$.

Hasimoto reconstructed the space curve from equation (15) by solving a Ricatti equation derived with the knowledge of κ and τ. The space curve is described as

$$\mathbf{x} = \begin{pmatrix} s - 2\frac{\mu}{\beta}\tanh\eta \\ 2\frac{\mu}{\beta}\,\mathrm{sech}\eta\,\cos\Theta \\ 2\frac{\mu}{\beta}\,\mathrm{sech}\eta\,\sin\Theta \end{pmatrix} \tag{16}$$

where $\eta = \beta(s - ct)$, $\mu = 1/(1 + T^2)$, $T = \tau/\beta$ and $\Theta = T\eta + (\beta^2 + \tau^2)t$. Figure 6 shows the perspective view of a curve described by solution (16) with $t = 0$, $\tau = 7.0$ and $\beta = 2.0$.

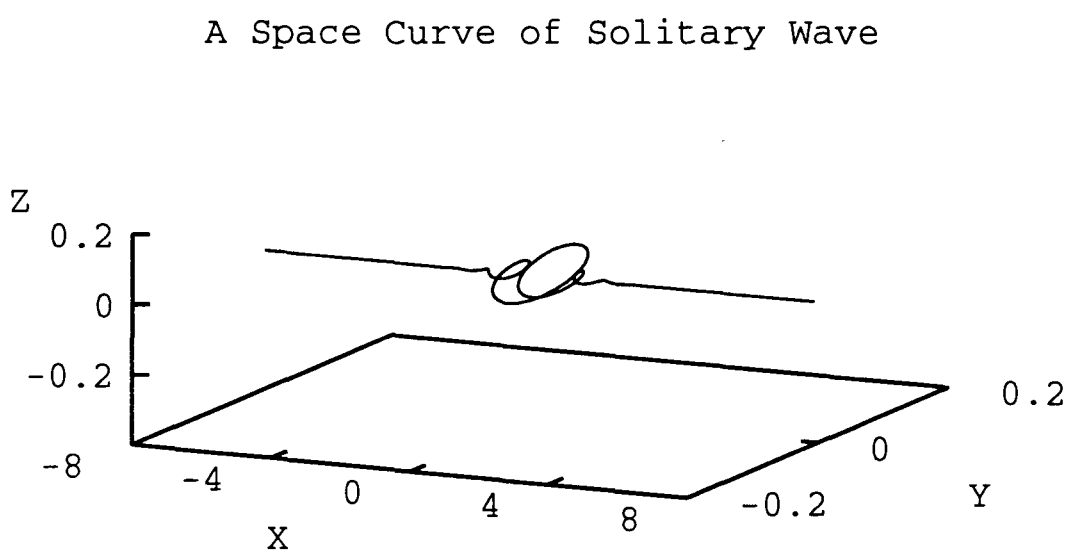

Figure 6: Perspective view of a space curve describing a solitary wave on a vortex filament

However, the question — whether there is a solitary wave solution on vortex filament in the Euler flow — remains. Because the LIA only describes the local

behavior of a vortex filament, and is lack of stretching — an important phenomenon of vortex dynamics (see Buttke [5]). A series of physical experiments was done by Hopfinger, Browand & Gagne [11], Maxworthy, Mory & Hopfinger [17] and Maxworthy, Hopfinger & Redekopp [16]. They reported the appearance of solitons on vortex core in their experiments. Aref & Flinchem attempted to answer this question numerically in their 1984 paper [1]. They concluded that 'in a shear, solitons cannot exist, but solitary waves can'. In their study, a solitary wave did not survive for long.

Now, with the help of the method described above, we indeed see the existence of solitons on vortex core in the Euler flow in our numerical experiments.

The initial data are generated from solution (16). The torsion τ in (16) and the core size σ for our numerical scheme are two very important facts for the simulation of solitons on a vortex tube.

Our numerical experiments show that for core size $\sigma < 0.1$, a computation becomes very unstable. That may be caused by the truncation error during the computation because for smaller σ, the exp function produces large value which may cause inaccuracy. Clearly σ should not be too large. (For more discussion about core size σ, one should see Qi [19, 18].)

We chose the value of σ between 0.1 and 0.5. For each fixed value of σ in [0.1, 0.5], there are certain values of τ at which we obtained stable results, that is, an initial solitary wave propagates along a vortex tube for a long time.

Figure 7 shows the motion of a soliton on a vortex filament. We only plot the middle part of our computation in these pictures. The perspective view of the initial data are shown in Figure 6. We used $\sigma = 0.3$ in our numerical computation. We computed 500 steps. From the last picture of Figure 7, we can see that the initial shape is very well preserved in spite of some dispersive waves. The solitary wave travels towards to the negative direction of x-axis. At the beginning, the center of the wave is at $x = 0$. After 500 steps computation, the wave center went somewhere near $x = -27$. We make two remarks for the simulation:

(1) With the same parameters we adopted for the initial data we used in our simulation, the solitary wave actually travels towards to the positive direction of x-axis in equation (16) which is a solution for the LIA. Therefore our numerical simulation can not match up the solution for the LIA quantitatively. As a matter of fact, the direction of the wave travels in our simulation can be changed for different choice of the parameters τ and σ.

(2) In Figure 7, the pictures at steps 40 and 50 shows an interesting phenomenon, i.e., the short length waves displayed in step 40 disappears at step 50. The long length wave such as the main wave we traced in our simulation is also stable. All the waves appeared in Figure 7 have the helical shape. Thus, the results of our numerical experiment disagree with the existing stability

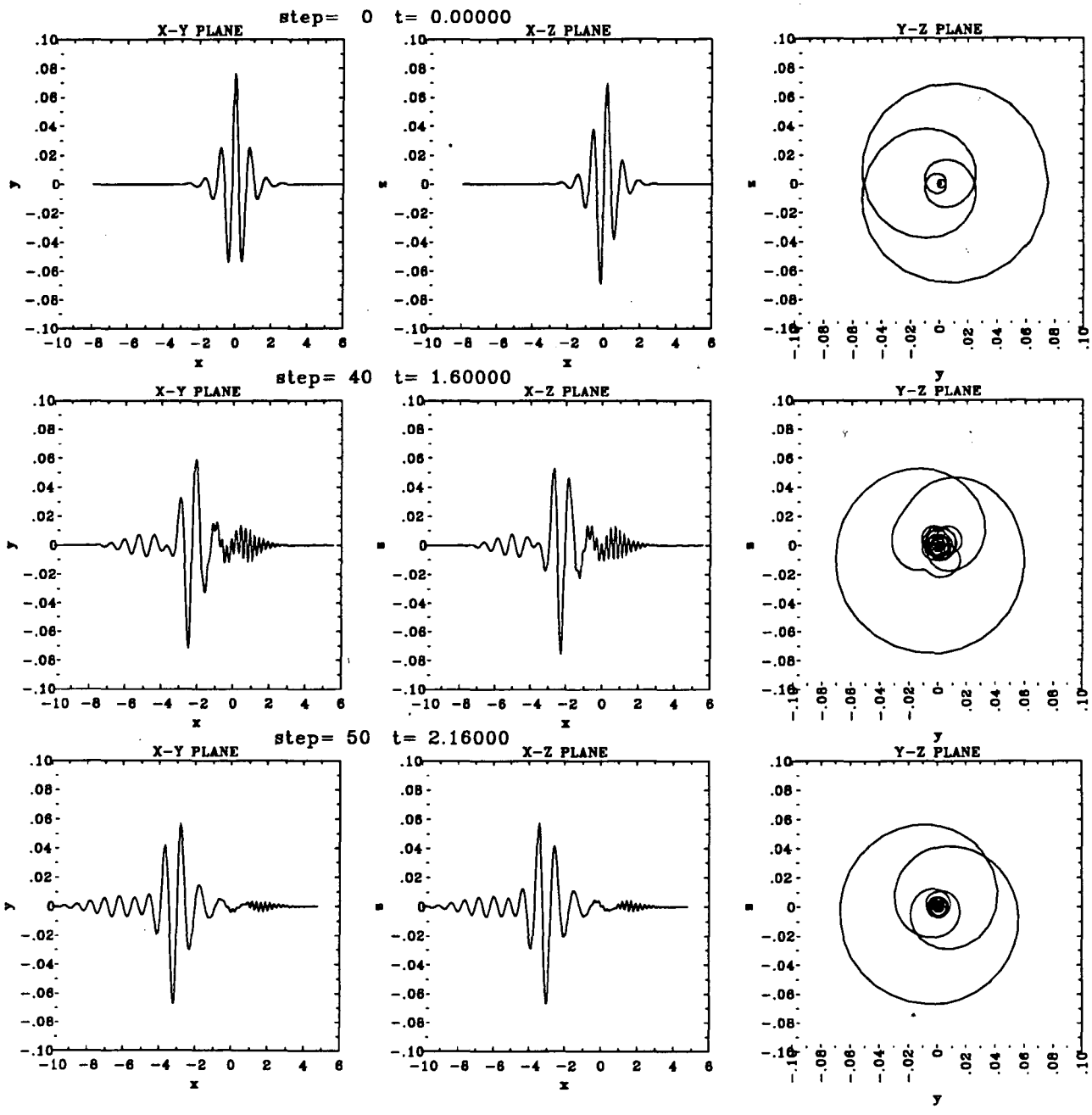
step= 0 t= 0.00000
X-Y PLANE
X-Z PLANE
Y-Z PLANE
step= 40 t= 1.60000
X-Y PLANE
X-Z PLANE
Y-Z PLANE
step= 50 t= 2.16000
X-Y PLANE
X-Z PLANE
Y-Z PLANE
x
y
z

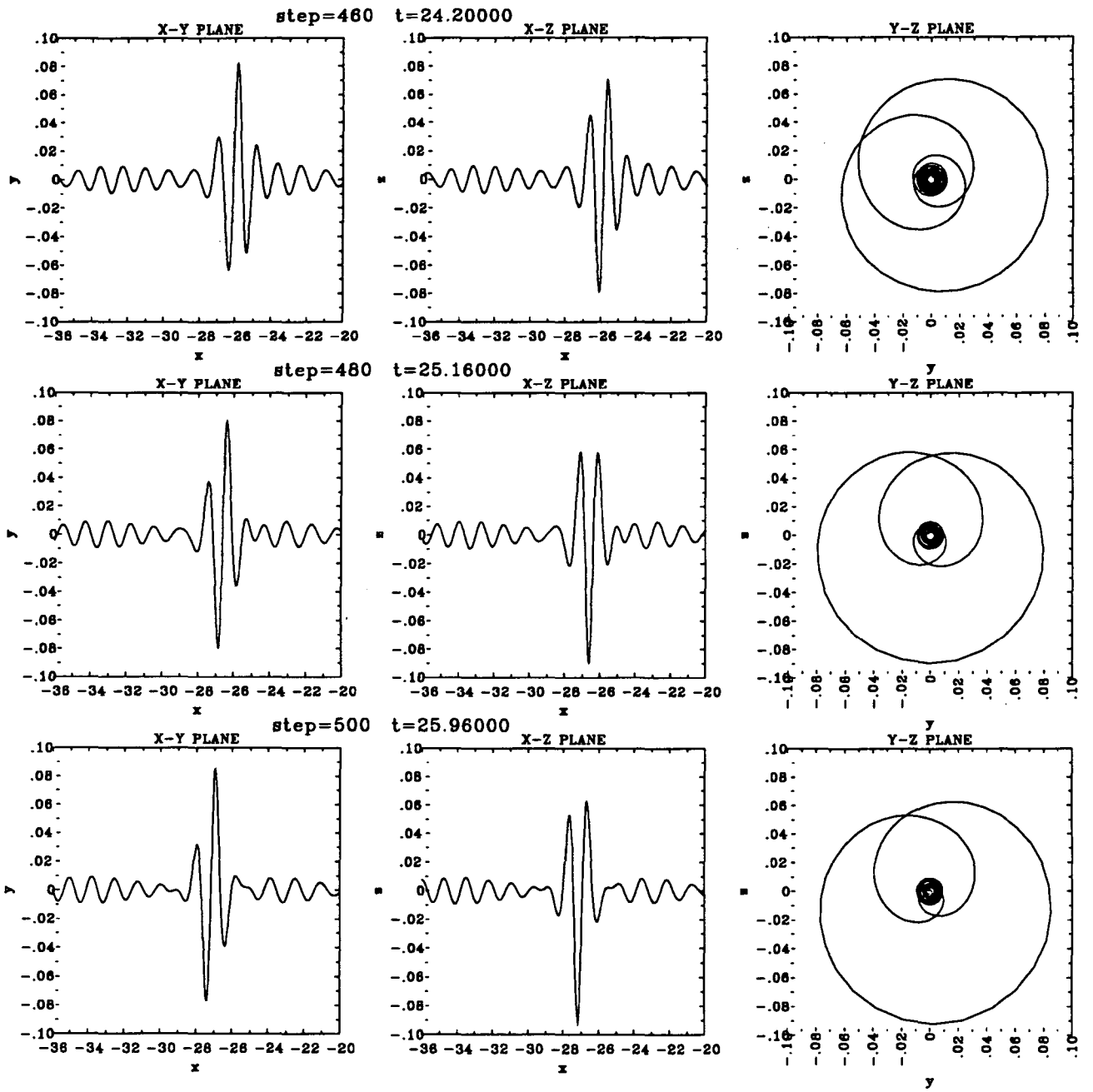

Figure 7: A solitary wave propagation on a vortex filament.

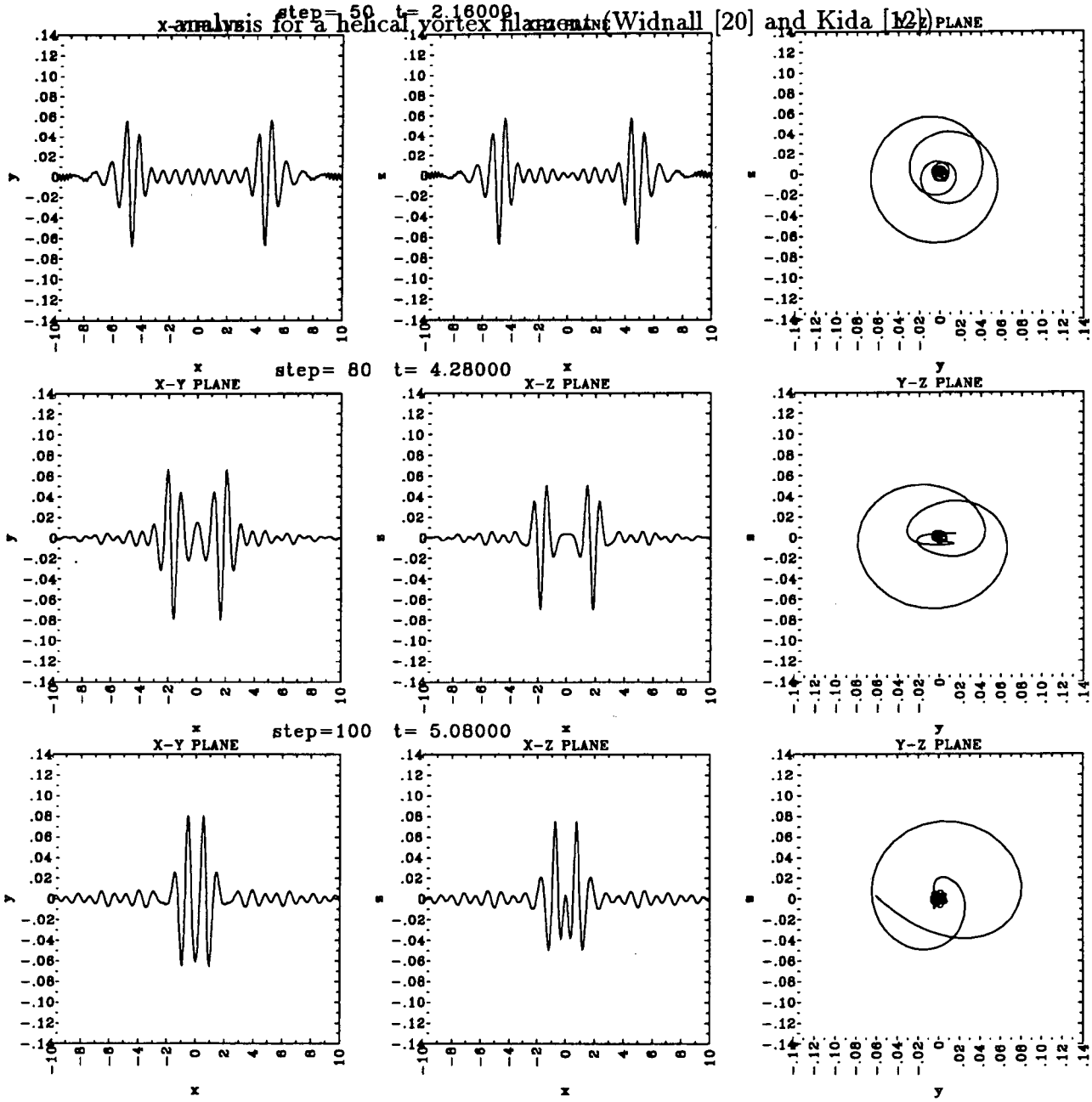

To confirm the wave motion shown in Figure 7 indeed a soliton, we should study the interaction of these waves. Figure 8 demonstrates the strong interaction (head on collision) of two mirror identical waves. The right wave is the same wave that we used in above simulation. From the pictures, one can clearly see that two waves collide together at step 110, then move away each other without 'scratching'. The strong interaction demonstrated here may not occur for some choices of τ and σ although for such choices, the shape can be preserved.

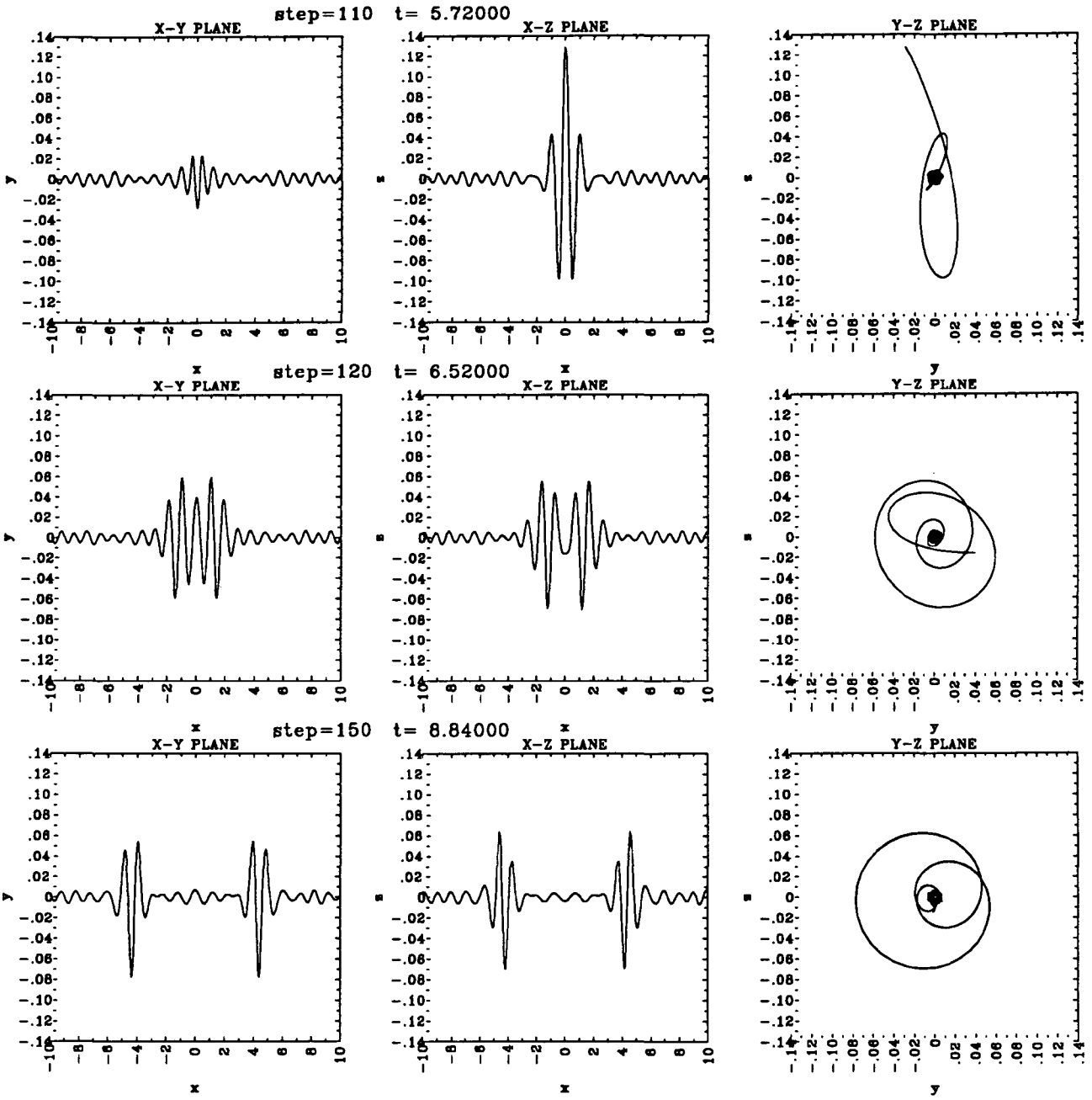

Figure 8: Collision of two solitons on a vortex filament.

5 Summary and discussion

We have described a three dimensional adaptive wave tracing vortex method. The adaptive wave tracing scheme is only for lines in this work. It should be easily extended to surfaces in three dimensional space, and be used for other particle methods as well.

We have given a detailed explanation for the numerical error introduced by choosing different lengths in different regions. Understanding such error and proper dealing with it are essential for accurate implementation of our scheme. The analysis also provides a hint for eliminating non physical stretching in a vortex computation.

As an application of the numerical scheme, we demonstrated a numerical simulation of a soliton propagating on a vortex filament and of the strong interaction of two mirror identical solitons. It is the first time, as author's knowledge, reported the successful numerical simulation of solitons on a vortex filament in the Euler flow. It indicates the possible integrable solutions for the Euler equations. Some of chaos phenomena and vortex stretching phenomenon are being studied and the results will be reported in a future paper.

Acknowledgments

The computation was carried out at the Lawrence Berkeley Laboratory. This work was supported in part by the Applied Mathematics Sciences subprogram of the Office of Energy Research, U.S. Department of Energy, under contract DE-AC03-76SF-00098, and in part by the National Science Foundation under grant number DMS89-19074.

References

[1] H. Aref and E.P. Flinchem. Dynamics of a vortex in a shear flow. *J. Fluid Mech.*, 148:477–497, 1984.

[2] R.J. Arms and F.R. Hama. Localized-induction concept on a curved vortex and motion of an elliptic vortex ring. *Phys. Fluids*, 8:553–59, 1965.

[3] G.K. Batchelor. *An Introduction to Fluid Dynamics.* Cambridge University Press, 1967.

[4] J.T. Beale and A. Majda. High order accurate vortex methods with explicit velocity kernels. *J. Comput. Math. Phys.*, 58:188–208, 1985.

[5] T.F. Buttke. A numerical study of superfluid turbulence in the Self-Induction Approximation. *J. Comput. Math. Phys.*, 76:301–326, 1988.

[6] A.J. Chorin. The evolution of a turbulent vortex. *Commun. Math. Phys.*, 83:517–535, 1982.

[7] P. G. Drazin and R. S. Johnson. *Solitons: An Introduction.* Cambridge University Press, 1989.

[8] F.R. Hama. Progressive deformation of a curved vortex filament by its own induction. *Phys. Fluids*, 5(10):1156–62, 1962.

[9] F.R. Hama. Progressive deformation of a perturbed line vortex filament. *Phys. Fluids*, 6(4):526–34, 1962.

[10] H. Hasimoto. A soliton on a vortex filament. *J. Fluid Mech.*, 51(3):387–98, 1972.

[11] E.J. Hopfinger, F.K. Browand, and Y. Gagne. Turbulence and waves in a rotating tank. *J. Fluid Mech.*, 125:505–534, 1982.

[12] S. Kida. Stability of steady vortex filament. *J. Phys. Soc. Japan*, 51:1655–1662, 1982.

[13] O.M. Knio and A.F. Ghoniem. Numerical study of a three-dimensional vortex method. *J. Comput. Math. Phys.*, 86:75–106, 1988.

[14] G.L. Lamb, Jr. *Elements of Soliton Theory.* John Wiley and Sons, 1980.

[15] A. Leonard. Computing three-dimensional incompressible flow with vortex elements. *Ann. Rev. Fluid Mech.*, 17:523–59, 1985.

[16] T. Maxworthy, E.J. Hopfinger, and L.G. Redekopp. Wave motions on vortex cores. *J. Fluid Mech.*, 151:141–165, 1985.

[17] T. Maxworthy, M. Mory, and E.J. Hopfinger. Waves on vortex cores and their relation to vortex breakdown. In *Proc. AGARD Conf. on Aerodynamics of Vertical Type Flows in Three-Dimensions.* AGARD CP 342, 1983. paper 29.

[18] A. Qi. Numerical studies of wave propagation on vortex filaments. submitted to *J. Comp. Phys.*

[19] A. Qi. *Three dimensional vortex methods for the analysis of wave propagation on vortex filaments.* PhD thesis, University of California at Berkeley, 1991.

[20] S. E. Widnall. The stability of a helical vortex filament. *J. Fluid Mech.*, 54:641–663, 1972.

LAWRENCE BERKELEY LABORATORY
UNIVERSITY OF CALIFORNIA
TECHNICAL INFORMATION DEPARTMENT
BERKELEY, CALIFORNIA 94720